Prediction of Atmospheric MTF and Application to Image Restoration, Based on Meteorological Data

3rd Quarterly Report

(May 1994)

Xeroxed

N. S. Kopeika, Principal Investigator

Department of Electrical and Computer Engineering

Ben-Gurion University of the Negev

Beer-Sheva, Israel

REPORT DOCUMENTATION PAGE

Form Approved OMB No. 0704-0188

1. AGENCY USE ONLY (Leave blank)	2. REPORT DATE	3. REPORT TYPE AND DATES COVERED
	Nay 1994	Final Report

4. TITLE AND SUBTITLE

Prediction of Atmospheric MTF and Application to Image Restoration, Based on Meteorological Data. 3rd Quarterly Report

5. FUNDING NUMBERS

F6170893W0896

6. AUTHOR(S)

I. Dror and N.S. Kopeika

7. PERFORMING ORGANIZATION NAME(S) AND ADDRESS(ES)

Ben Gurion University of the Negev
Department of Electrical and Computer Engineering
Beer Sheva, Israel 84105

8. PERFORMING ORGANIZATION REPORT NUMBER

SPC-93-40603

9. SPONSORING/MONITORING AGENCY NAME(S) AND ADDRESS(ES)

EOARD
PSC 802 BOX 14
FPO 09499-0200

10. SPONSORING/MONITORING AGENCY REPORT NUMBER

SPC-93-4060

11. SUPPLEMENTARY NOTES

12a. DISTRIBUTION/AVAILABILITY STATEMENT

Approved for public release; distribution is unlimited.

12b. DISTRIBUTION CODE

A

13. ABSTRACT (Maximum 200 words)

Predictions of atmospheric transmittance in desert aerosol environments using MODTRAN code diverge significantly from measured data. Good prediction of the desert particulate size distribution is required in order to predict atmospheric scattering and absorption parameters. It is also essential to the prediction of the aerosol atmospheric modulation transfer function which is often the dominant component of the overall atmospheric MTF. Recently an effort to predict statistics but not size distribution according to simple weather parameters has been made for coarse desert aerosols. A quantitative analysis of the desert particulate size distribution models was also performed. In this research, the size distribution parameters measured by optical counters are related to weather parameters. Known statistical and analytical models such as MODTRAN relate the size distribution parameters only to relative humidity for continental atmospheres. Although humidity has a significant role in the prediction of aerosol size statistics, other weather parameters are seen here to strongly influence also the size distribution parameters. Comparisons such as the above can be used to predict under which conditions the MODTRAN aerosol models have good or poor accuracy. It is also hoped that they will lead to improvements in MODTRAN, improving the accuracy of the humidity dependence as well as by incorporating other meteorological parameters into the MODTRAN prediction models.

14. SUBJECT TERMS	15. NUMBER OF PAGES
	16. PRICE CODE

17. SECURITY CLASSIFICATION OF REPORT	18. SECURITY CLASSIFICATION OF THIS PAGE	19. SECURITY CLASSIFICATION OF ABSTRACT	20. LIMITATION OF ABSTRACT
UNCLASSIFIED	UNCLASSIFIED	UNCLASSIFIED	UL

Prediction of Atmospheric MTF and Application to Image Restoration, Based on Meteorological Data

Third Quarterly Report

This quarter work continued once again on image restoration, and on aerosol size distribution prediction.

The image restoration was primarily in the 3 - 5 μm wavelength region and is described in *Appendix 1*. What is notable is that the restoration work, based on atmospheric MTF, used *prediction* of turbulence MTF instead of direct measurement. Furthermore, it was found that, contrary to common impressions, high spatial frequency filtering does not necessarily bring about improved image quality. It is necessary to include in the atmospheic MTF modelling the unique shape of the aerosol MTF. It is shown here that high spatial frequency filtering without considering the unique MTF *shape* of such image degradation is not nearly as effective as when such shape is considered. Such examples are included in Appendix 1.

The key to aerosol MTF prediction is aerosol size distribution prediction. A model for relatively low humidity conditions (our summer) has indeed been developed now and is included here as *Appendix 2*. It is relevant to most weather situations, except for extreme ones such as duststorms or very high humidity situations. Efforts are continuing now to extend it to high humidity situations (our winter) for the next report. The present model indicates very high correlation of prediction with experiment except for such extreme conditions, as shown in typical examples in Appendix 2.

APPENDIX 1

Restoration of thermal images distorted by the atmosphere, using predicted atmospheric modulation transfer function

D. Sadot, G. Lorman, R. Lapardon, and N. S. Kopeika

Department of Electrical and Computer Engineering

Ben-Gurion University of the Negev

Beer-Sheva, Israel

Abstract

Restoration of thermal images distorted by the atmosphere, detected with a focal plane array (FPA) Pt-Si thermal imaging system, is presented. The restoration method is based upon atmospheric modulation transfer function (MTF) analysis. Using turbulence and aerosol MTF prediction models, atmospheric distortions and image degradation are modeled. Restoration results indicate significant improvement in image quality. However, it is critical to include the unique shape of aerosol MTF when modeling atmospheric MTF in order to obtain good restoration.

Introduction

Thermal imaging systems have progressed significantly in recent years. New focal plane array technology similar to ccd arrays in the visible range permits high resolution imaging. However, when dealing with long distance imaging through the atmosphere, system performance is often limited due to the atmospheric distortions. Usually, the atmospheric effect in the thermal range is referred to in target acquisition models[1] as a constant attenuation via the Beer-Lambert law. No treatment is considered for the spatial frequency dependence of the atmospheric effect i.e., the atmospheric thermal imaging MTF (primarily aerosol MTF).[2,3] However, recent analysis[2,3],applying some practical instrumentation limitations to the "classical" theory,[4] predicts significant atmospheric MTF variation with spatial frequency in the thermal range too. Knowledge of atmospheric MTF is essential to real-time high-resolution image restoration.

Results of measured atmospheric MTFs in the long wave 8-12 μm thermal range with low resolution imagers are shown elsewhere,[2,3] and are in good agreement with theoretical predictions. Here, turbulence and aerosol MTFs in the 3-5 μm wavelength atmospheric window with higher resolution imagers are estimated using both turbulence[5] and aerosol MTF prediction models, with the knowledge of standard meteorological parameters. Based on atmospheric MTF, restoration of images recorded along horizontal atmospheric paths is presented, indicating significant improvement in image resolution. This demonstrates the wide variety of applications that are achievable on the basis of atmospheric MTF analysis in the infrared.

Experiment

The thermal IR imaging system used was a CCD6003 Platinum Silicide Infrared Television Camera. It incorporates a 488 x 512 element infrared CCD (IRCCD) image sensor

designed to provide general-purpose passive day/night imaging capability. Sensor spectral band is 3-5 μm. The camera is equipped with a 100 mm focal length lens with a 6.9 (V) x 9.2 (H) degrees field-of-view. An optional 500 mm focal length lens is available too. Camera integration time is 1/30 second. All video signals were digitized via a Matrox frame grabber and recorded on a personal computer for further analysis. Images were recorded through an open laboratory window at an altitude of about 15 meters above the ground, horizontally, for image paths between 2 to 7 km. The receiver was located on stable marble optical tables located inside the laboratory, thus minimizing significantly any possible mechanical vibrations.

During the experiment, measurements were taken of standard meteorological data - ambient temperature, relative humidity, solar flux, wind speed, and particle size distribution. The latter were measured over 0.16 to 10 μm particulate radius using Particle Measurement System Inc. (PMS) instrumentation . .

Simultaneously, natural and urban ground scenes along the line-of-sight were recorded, containing blur caused by atmospheric distortions.

Using the *predicted Atmospheric MTF*, image restoration techniques were applied to the distorted images, improving significantly image quality.

Prediction models

A model for predicting turbulence MTF already exists[5] (verified independently by U.S. Army Night Vision Laboratory). Also available are IMTURB or PROTURB (U.S. Army Atmospheric Sciences Lab.). With the knowledge of standard meteorological parameters such as ambient temperature, relative humidity, wind speed, and solar flux, the turbulence strength parameter C_n^2 can be predicted quite accurately. Using C_n^2 prediction, both short and long exposure turbulence MTFs[6] can be evaluated.

In principle, the knowledge of aerosol size distribution and refractive index, together with instrumentation parameters, can be used to predict aerosol MTF.[4] In Fig. 1, a typical

aerosol size distribution during the time the experiment was carried out is presented. For particulates of radii smaller than 0.16 μm, size distribution was extrapolated according to the Air Force Geophysics laboratory model[7], since these could not be measured with this PMS instrumentation. Mie phase function was calculated according to the aerosol size distribution. Fig. 2 presents aerosol phase function corresponding to the size distribution of Fig. 1. The scattering and absorption coefficients were evaluated too according to Mie theory.[8] The medium's Mie parameters, together with instrumentation parameters including field-of-view, spatial frequency bandwidth, sensor's dynamic range, and scene's target to background SNR, were applied to the *Practical Aerosol MTF* model.[4] Results of this analysis are presented in the following figures. First, the imaging system MTF is presented in Fig. 3. In Fig. 4 the "classical" aerosol MTF together with the system MTF are presented on a log-log scale. Fig. 5 presents the Specific Intensity Function, which is the Radiative Transfer Equation solution, but limited according to system MTF. According to Fig. 5 the ratio between the unscattered and scattered components of light actually recorded in the image is relatively small, unlike the "classical" model prediction.[9] The latter refers to the unscattered light as an angular delta function, thus predicting extremely higher value to the unscattered-to-scattered light intensity ratio. The reduction of the ratio of the unscattered to scattered light actually recorded in the image is due to the system's spatial frequency bandwidth limitation. This limitation causes a severe blur of unscattered light, reducing this ratio to only *one* order of magnitude, in comparison to an angular delta function as predicted by "classical" theory. In Fig. 6 is an example of the *Detected* Specific Intensity Function for particulate light scatter after applying all the imaging system limitations (including finite field of view, dynamic range and received SNR). This represents an atmospheric aerosol point spread function much narrower than that predicted by classical aerosol MTF theory and is due to the instrumentation which narrows by several orders of magnitude the angles of light scatter actually recorded in the image from that incident to the receiver.[4] The final result of *Practical* aerosol MTF theory is presented in Fig. 7 (continuous line). In addition, presented also are the system (dashed) and turbulence (dotted)

MTFs. Turbulence MTF was predicted using the prediction model[5] mentioned above, with the use of meteorological data measured during the experiment. All three MTFs are multiplied in order to obtain the overall system and atmospheric MTF. This overall MTF for 6.5 km distance is presented in Fig. 8 and is the MTF used for further image restoration analysis for the objects located at that range.

Image restoration

Enhancement techniques for thermal images are summarized elsewhere.[10] Here, we will concentrate on deblurring atmospheric effects.

Using the predicted thermal IR atmospheric MTF, several filtering techniques were applied to some thermal images recorded by the same imaging system in order to restore the blurred images. The most successive restorations were obtained by using Wiener[11] and Improved Wiener[12] filters. Other spatial frequency filters, such as inverse and pseudo-inverse filters, achieved less successful results. Fig. 9 presents an image recorded by the IRCCD camera equipped with a 100 mm focal length lens. The upper part of the scene includes buildings at a distance of 1.5 km. Atmospheric turbulence was moderate and the atmosphere was relatively clear from particulates over the relatively short pathlength. Thus it is assumed that most of the image blur was caused by the imaging system MTF. In Fig. 10 is the restored image using the standard Wiener filter technique. Though image degradation was not severe as explained above, there is a distinct improvement in image quality after restoration. A good indication of this is the windows in the remote buildings at the top which are clearly sharpened.

In general, if the noise was negligible, the Wiener filter would have reduced to an inverse filter. However, for any practical system, including imaging systems and the atmosphere, its transfer function goes to zero at high spatial frequencies, so the inverse filter will approach infinity at high spatial frequencies. Since any practical image contains noise, the Wiener filter limits image enhancement at high spatial frequencies so as to prevent infinite

noise enhancement in the restored image. This is demonstrated in Fig. 11, which represents the standard Wiener filters for different SNRs, such as used in the restoration of Fig. 9.

When atmospheric conditions become worse or, conversely, over longer distances, atmospheric limitations dominate. Such an example is demonstrated in Fig. 7 where, for an optical pathlength of 6.5 km, turbulence and aerosol MTFs are much more severe than the system MTF. An example of a recorded image in the IRCCD camera equipped with a 500 focal length lens, through an optical pathlength of 6.5 km, is presented in Fig. 12. Predicted turbulence and aerosol MTFs are very similar to those presented in Fig. 7. Restoration of the image of Fig. 12 using the improved Wiener filter is presented in Fig. 13. Very similar results yielding almost same image quality were obtained using the standard Wiener filter. This is not surprising since the improved Wiener filter is based upon modeling correctly the relative part of image degradation caused by turbulence jitter, as explained in Ref. 12. However here, due to relatively low angular spatial frequencies (up to 7800 cycles/radian), and weak turbulence strength (about $3 \cdot 10^{-15}$ $[m^{-2/3}]$), turbulence jitter contribution to image degradation is weak. Therefore, both standard Wiener and improved Wiener filters yield almost the same results.

Quantitative investigation of image correction is demonstrated in Fig. 14. The dashed curve represents the overall (system and atmospheric) predicted MTF for the image of Fig. 12. The dashed-dotted curve represents the improved Wiener filter used to obtain the restored image of Fig. 13. The continuous curve represents the *restored overall MTF* obtained after image correction. Improvement of image quality, especially at high spatial frequencies is obvious, thus improving significantly image resolution. This means that essentially most atmospheric blur is removed in the restoration process, and the distant object scene is observed as if there were almost no atmosphere.

A very important issue is the restoration sensitivity to blur estimation model. As explained previously, the blur model includes three components; turbulence MTF, practical aerosol MTF, and hardware MTF (Fig. 7). Failure in modeling correctly one of the three

components will limit the quality of the restored image. Often researchers have the impression that most high spatial frequency filtering yields some image restoration. This is not true. It is critical to consider the unique shape and cutoff frequency of aerosol MTF. Here, examples of Wiener filter restoration of the scene in Fig. 9, using inaccurate MTF estimations, are presented. MTF estimations were of a Gaussian form, with varying cutoff spatial frequencies:

$$\hat{MTF} = \exp\left(-\frac{\Omega^2}{\Omega_c^2}\right) \qquad (1)$$

where $\hat{MTF}$ is the Gausian MTF estimator, Ω is angular spatial frequency [cycles·rad^{-1}], and Ω_c is the estimator cutoff frequency. In Fig. 15a, the overall blur MTF estimation is of a Gausian form with a cutoff frequency of 1300 [cycles/radian]. In Fig. 15b, a similar estimator is used with a cutoff frequency of 4300 [cycles/rad]. It is obvious that in both "restorations" image quality was *reduced* instead of being restored. Repeating the restoration process with other Gausian-form MTF estimators of varying cutoff frequencies yielded best restoration results with a cutoff frequency of 2300 [cycles/rad]. The restored image is presented in Fig. 16. Indeed, the best Gausian estimator was most similar to the actual predicted atmospheric and system MTF (of Fig. 8, using turbulence and aerosol MTF prediction models). A comparison between the Gausian and actual predicted MTFs is presented in Fig. 17. For the Gausian estimator, restoration was fairly good but not as well as the restoration in Fig. 13, which is based on the actual atmospheric MTF prediction model. This comparison is also a good validation to the MTF prediction model since the best MTF prediction model yields best image restoration. In addition, prediction and restoration procedure is implemented in real-time, saving a lot of time for trial-and-error estimation techniques of other image sharpening algorithms in order to estimate correctly the cutoff frequency of the blurring MTF. Prediction can only be possible by considering the atmospheric MTF properly, including the significant role played by aerosol MTF. Restoration based on MTF does not depend on target shape. It is a fundamental image correction, which can be followed by other image processing techniques as required. Knowledge of the atmospheric MTF including aerosol MTF permits faster image correction without the need for many iterations.

Conclusions

Restoration of thermal images distorted by the atmosphere, recorded with an IRCCD camera, is presented. Restoration is based upon spatial frequency filters deriving from the knowledge of the thermal IR atmospheric MTF. Such restoration is fundamental and yields image quality limited essentially by hardware, as if there were almost no atmosphere. This is in contradiction to the conventional approach, which usually regards the atmospheric effect in the IR range as attenuation only with no spatial frequency dependence considered. In principle, atmospheric MTF can be predicted according to weather forecast, and implemented in image restoration accordingly. This is important when dealing with *real-time* image restoration so that processing time is limited to computational time only, with no need for simultaneous atmospheric measurements. Knowledge of atmospheric MTF is essential to good cost-effective system design and is very useful in image restoration without any prior knowledge of the target to be viewed.

References

1. S. R. Rotman, E. S. Gordon, and M. L. Kowalcyzk, "Modeling human search and target acquisition performance: 3. Target detection in the presence of obscurants," *Optical Engineering*, **30**, No. 6, pp. 824-829, June 1991.
2. D. Sadot and N. S. Kopeika "Thermal imaging through the atmosphere: Atmospheric MTF theory and verification," *Optical Engineering*, **33**, No. 3, pp. 881-888, March 1994.
3. D. Sadot, A. Dvir, I. Bergel and N. S. Kopeika, "Restoration of thermal images distorted by the atmosphere, based upon measured and theoretical atmospheric modulation transfer function," *Optical Engineering*, **33**, No. 1, pp. 44-53, January, 1994.
4. D. Sadot and N. S. Kopeika, "Practical instrumentation-based theory and verification of aerosol MTF," *J. Opt. Soc. of Amer. A,* **10**, No. 1, pp. 172-179, January 1993.
5. D. Sadot and N. S. Kopeika, "Forecasting optical turbulence strength on the basis of macroscale meteorology and aerosols: models and validation," *Optical Engineering*, **31**, No. 2, pp. 202-212, February, 1991.
6. J. W. Goodman, *Statistical Optics*, (Wiley, New York, 1985).
7. R. W. Fenn, S. A. Clough, W. O. Gallery, R. E. Good, F. X. Kneizys, J. D. Mills, L. S. Rothman, E. P. Shettle, and F. E. Volz, *Handbook of geophysics and space environment*, Air Force Geophysics laboratory, Chapter 18, Hanscom AFB, NTIS (1985).
8. M. Kerker *The scattering of light and other electromagnetic radiation*, Academic Press, 1969.
9. A. Zardecki, S. A. W. Gerstl, and J. F. Embury, "Multiple scattering effects in spatial frequency filtering," *Applied Optics*, **23**, No. 22, pp. 4124-4131, November, 1984.

10. J. Silverman and V. E. Vickers, "Display and enhancement of infrared images," in *Electro-Optical Displays,* M. A. Karim, ed., Marcel Dekker, Inc., New York, 1992, pp. 585-651.

11. A. Rosenfeld, and A. C. Kak, *Digital picture processing*, Academic Press, London, 1976.

12. D. Sadot, A. Rosenfeld, G. Shuker, and N. S. Kopeika, "High resolution restoration of images distorted by the atmosphere, based upon average atmospheric MTF," submitted for publication.

Figure Captions

Fig. 1. Atmospheric particle size distribution. S_a and A_a are scattering and absorption coefficients respectively at 4 μm wavelength.

Fig. 2. Medium's phase function.

Fig. 3. MTF of the IRCCD.

Fig. 4. Aerosol ("classical" model) together with imaging system MTF.

Fig. 5. Specific intensity function (Radiative Transfer solution) for the aerosol size distribution of Fig. 1, based on system MTF of Fig. 3.

Fig. 6. Detected (dashed) and "classical" (continuous) specific intensity functions for aerosol MTF.

Fig. 7. Comparison between practical aerosol (continuous), turbulence (dotted), and imaging system (dashed) MTFs.

Fig. 8. Overall atmospheric and system MTF.

Fig. 9. Original picture recorded by the IRCCD camera equipped with the 100 mm focal length lens. The remote buildings are at a distance of 1.5 km.

Fig. 10. Restoration of the original image of Fig. 9.

Fig. 11. The standard Wiener Filters as used in Fig. 10. From upper to lower curve SNR = 67, 33, 21, and 16, respectively.

Fig. 12. Original picture recorded by the IRCCD camera equipped with the 500 mm focal length lens. The object is located at a distance of 6.5 km.

Fig. 13. Restoration of the original image of Fig. 11.

Fig. 14. Comparison between the overall (dashed) and restored (continuous) MTFs, and the *improved wiener filter* (dash-dotted).

Fig.15a-b. Restorations of the original image of Fig. 12, using Gausian blur model estimation with different cutoff spatial frequencies; a) cutoff frequency of 1300 [cycles/rad]. b) cutoff frequency of 4300 [cycles/rad].

Fig. 16. Same as Fig. 15, for a Gausian MTF estimator with a cutoff frequency of 2300 [cycles/rad].

Fig. 17. Comparison between atmospheric MTF prediction model (dashed) and best Gausian estimator (continuous).

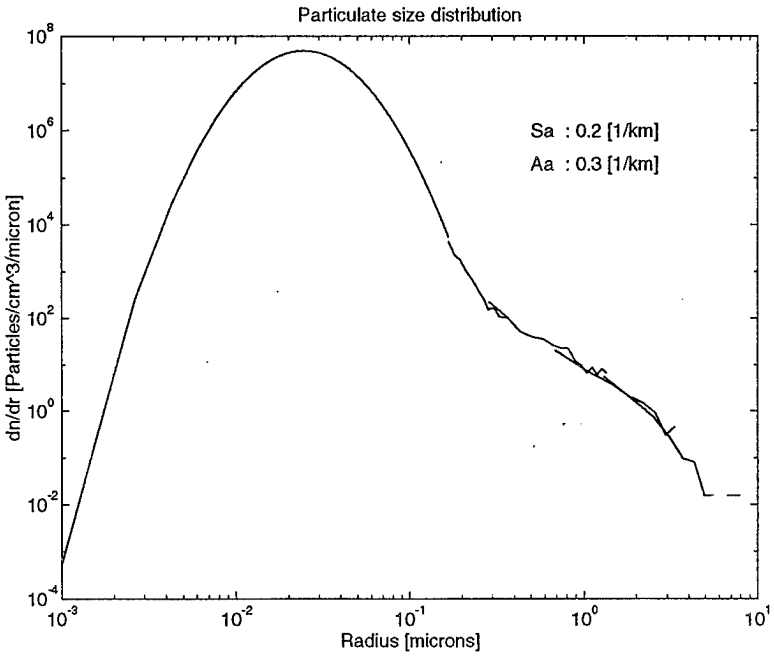
Particulate size distribution
Sa : 0.2 [1/km]
Aa : 0.3 [1/km]
dn/dr [Particles/cm^3/micron]
Radius [microns]

Fig. 1

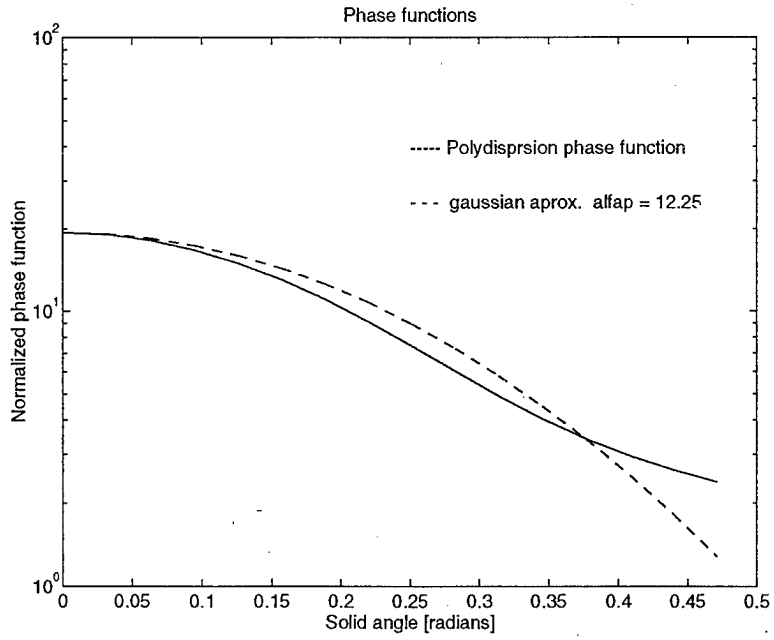
Phase functions
----- Polydisprsion phase function
- - - gaussian aprox. alfap = 12.25
Normalized phase function
Solid angle [radians]

Fig. 2

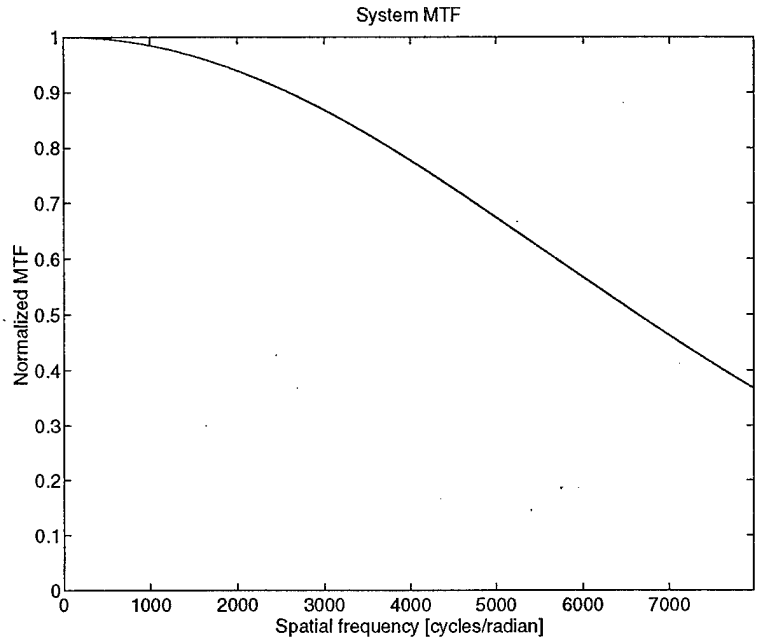
System MTF
Normalized MTF
Spatial frequency [cycles/radian]
0
0.1
0.2
0.3
0.4
0.5
0.6
0.7
0.8
0.9
1
0
1000
2000
3000
4000
5000
6000
7000

Fig.3

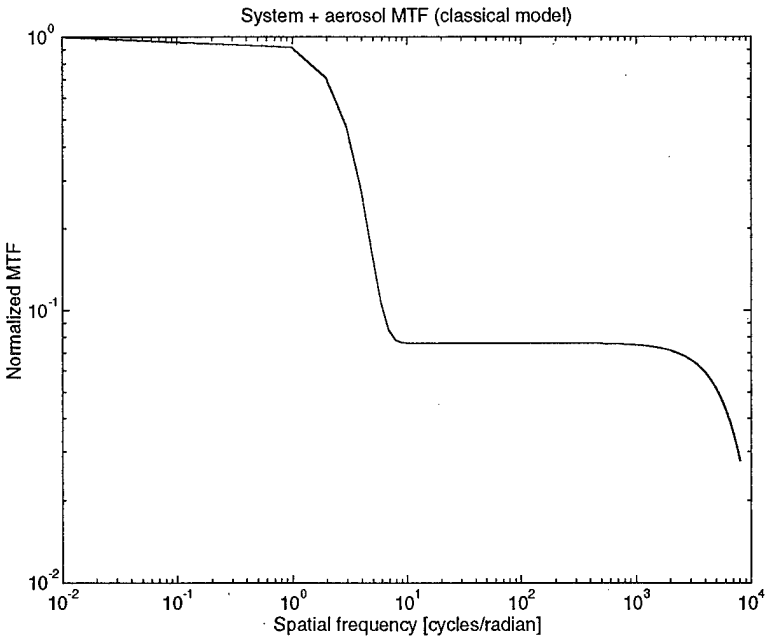
System + aerosol MTF (classical model)
Normalized MTF
Spatial frequency [cycles/radian]
10^{0}
10^{-1}
10^{-2}
10^{-2}
10^{-1}
10^{0}
10^{1}
10^{2}
10^{3}
10^{4}

Fig. 4

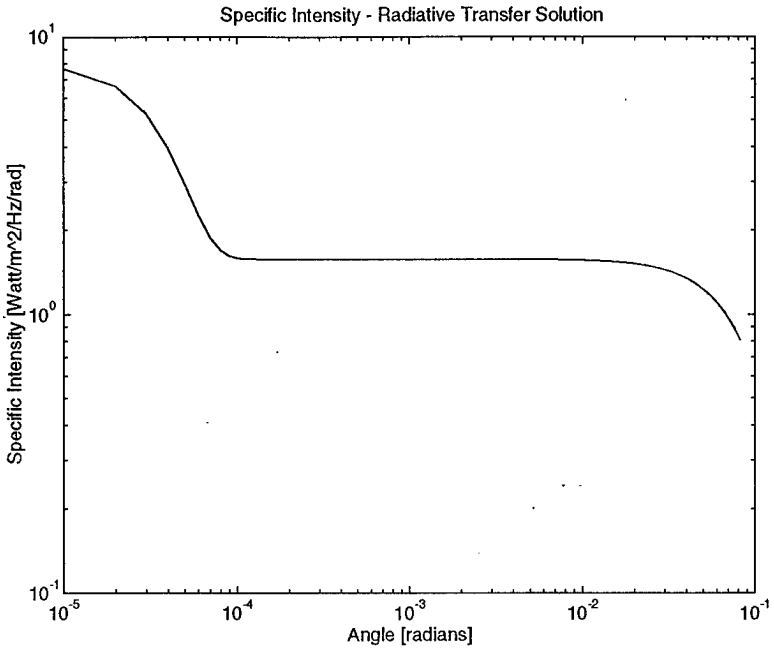
Specific Intensity - Radiative Transfer Solution
Specific Intensity [Watt/m^2/Hz/rad]
Angle [radians]

Fig. 5

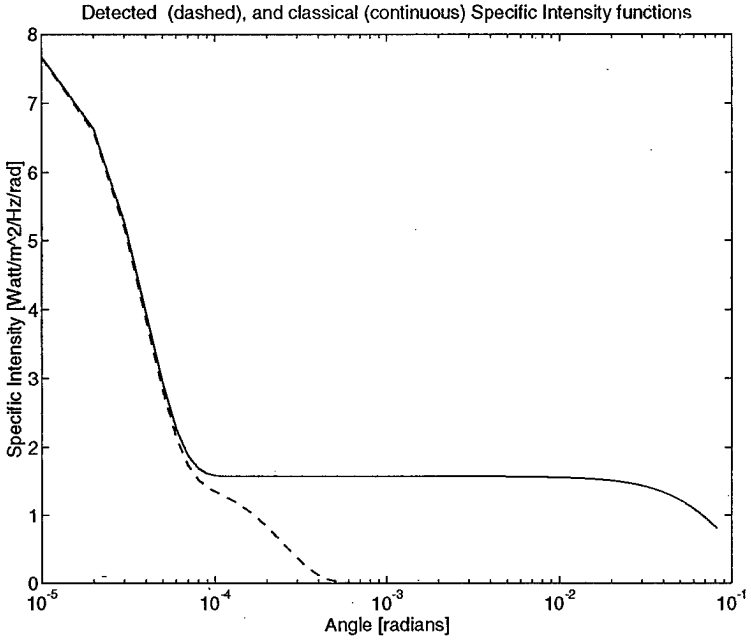
Detected (dashed), and classical (continuous) Specific Intensity functions
Specific Intensity [Watt/m^2/Hz/rad]
Angle [radians]

Fig. 6

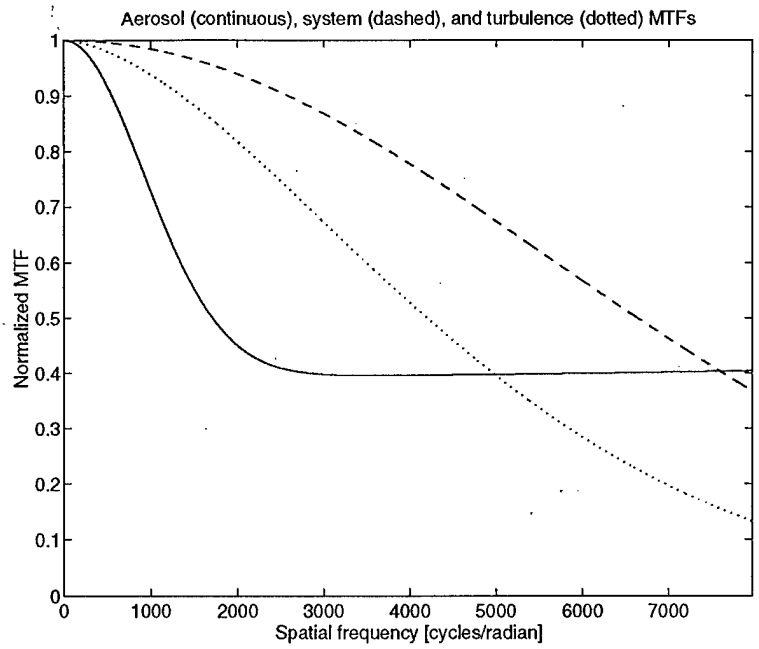
Aerosol (continuous), system (dashed), and turbulence (dotted) MTFs
Normalized MTF
Spatial frequency [cycles/radian]
0
0.1
0.2
0.3
0.4
0.5
0.6
0.7
0.8
0.9
1
0
1000
2000
3000
4000
5000
6000
7000

Fig. 7

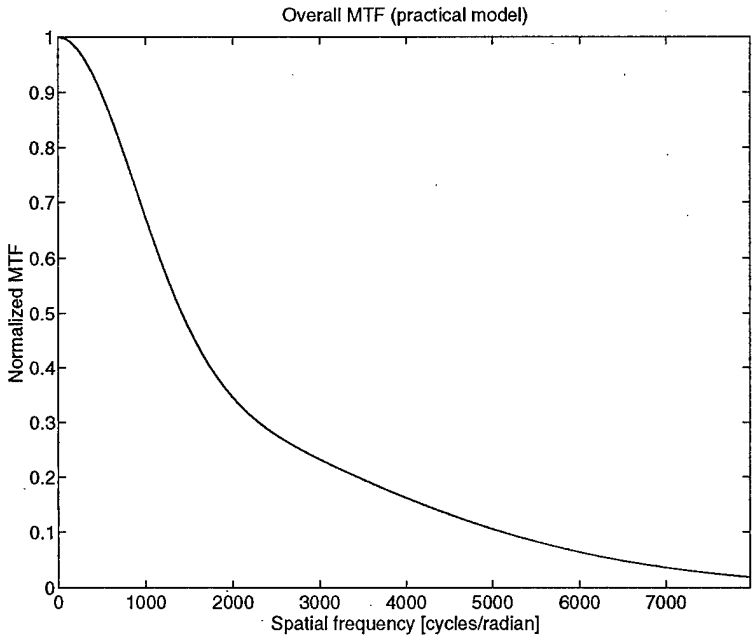
Overall MTF (practical model)
Normalized MTF
Spatial frequency [cycles/radian]
0
0.1
0.2
0.3
0.4
0.5
0.6
0.7
0.8
0.9
1
0
1000
2000
3000
4000
5000
6000
7000

Fig. 8

Original picture

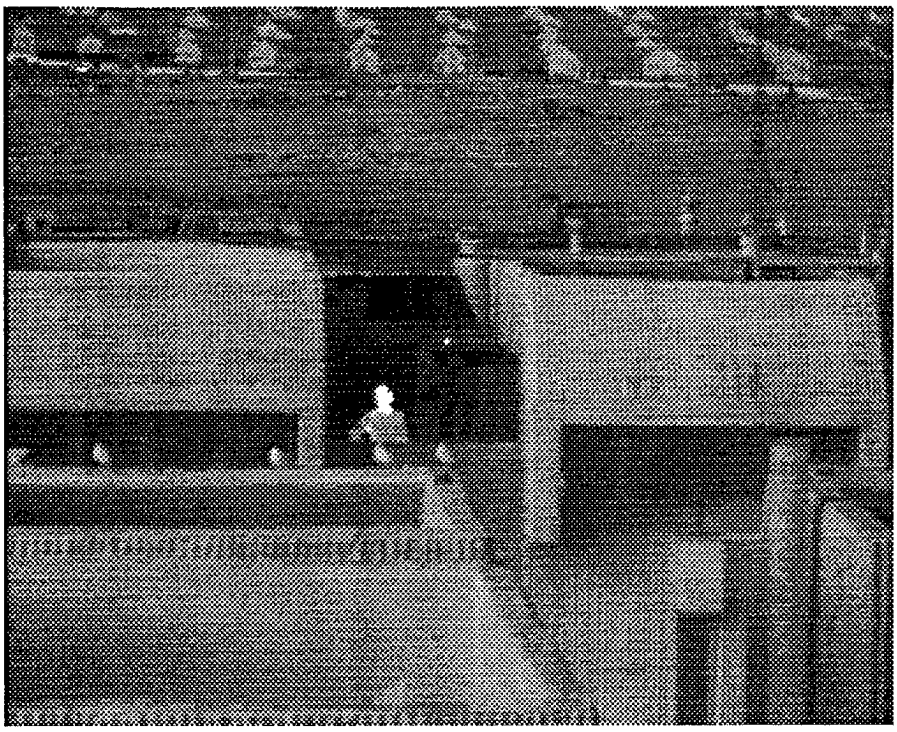

Fig. 9

Wiener filter

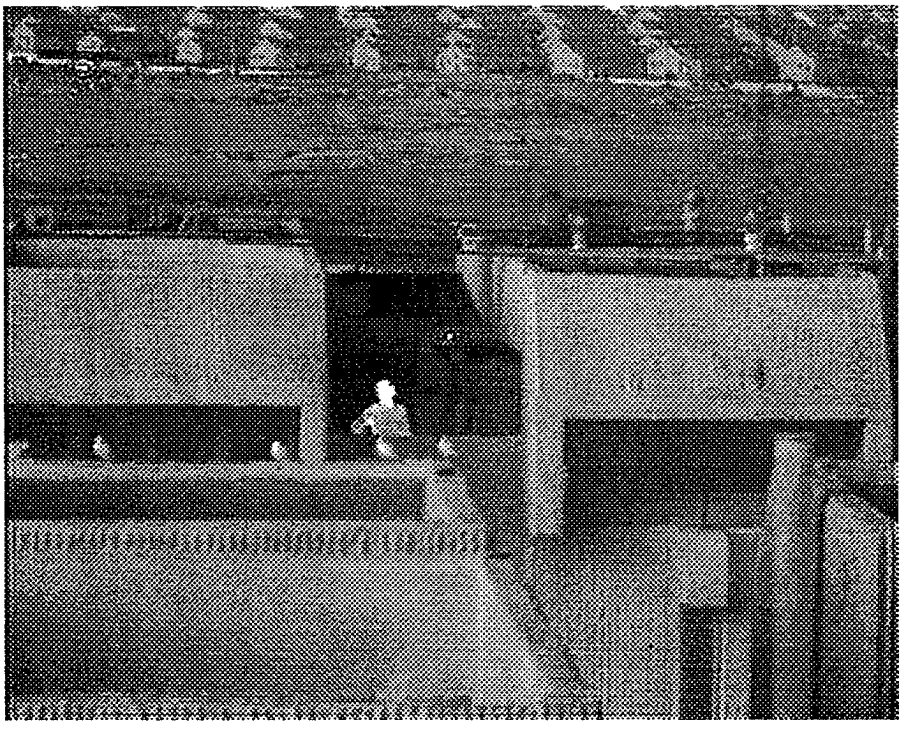

Fig. 10

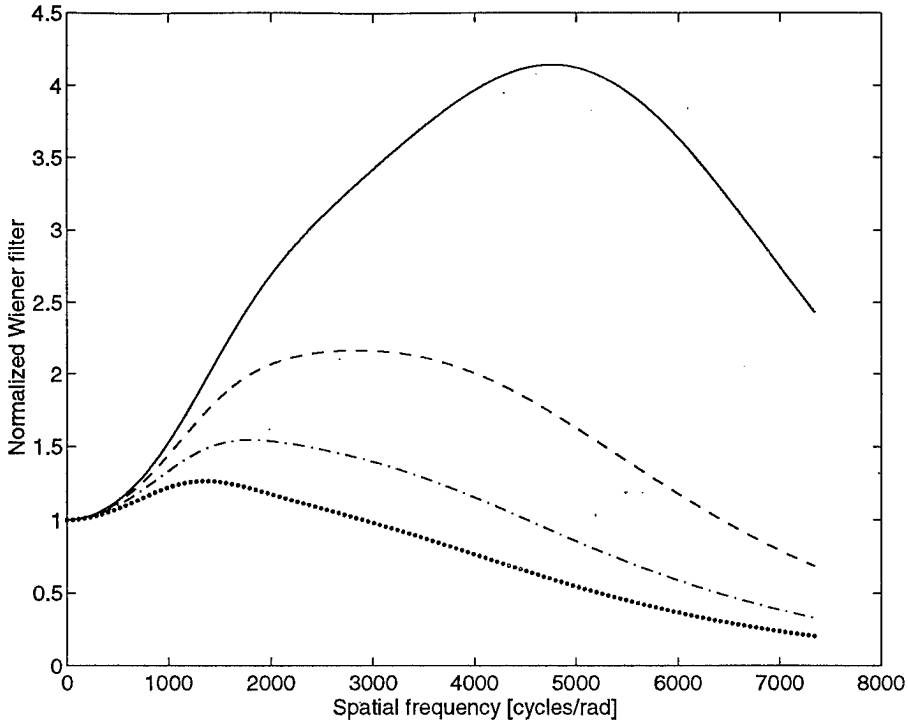
Normalized Wiener filter
Spatial frequency [cycles/rad]
0
0.5
1
1.5
2
2.5
3
3.5
4
4.5
0
1000
2000
3000
4000
5000
6000
7000
8000

Fig. 11

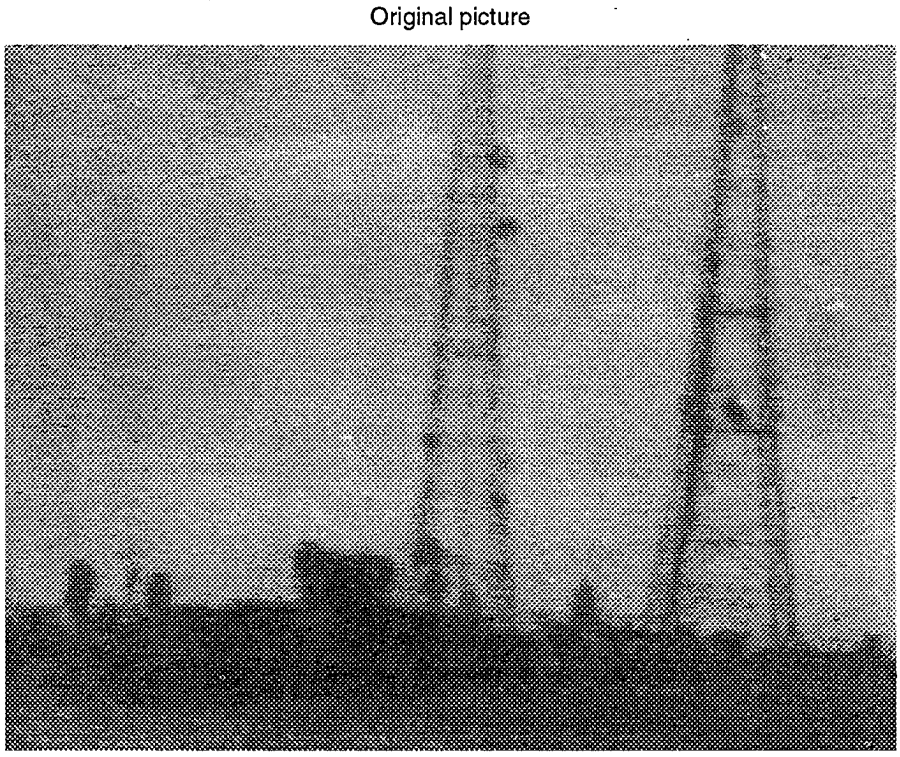
Original picture

Fig. 12

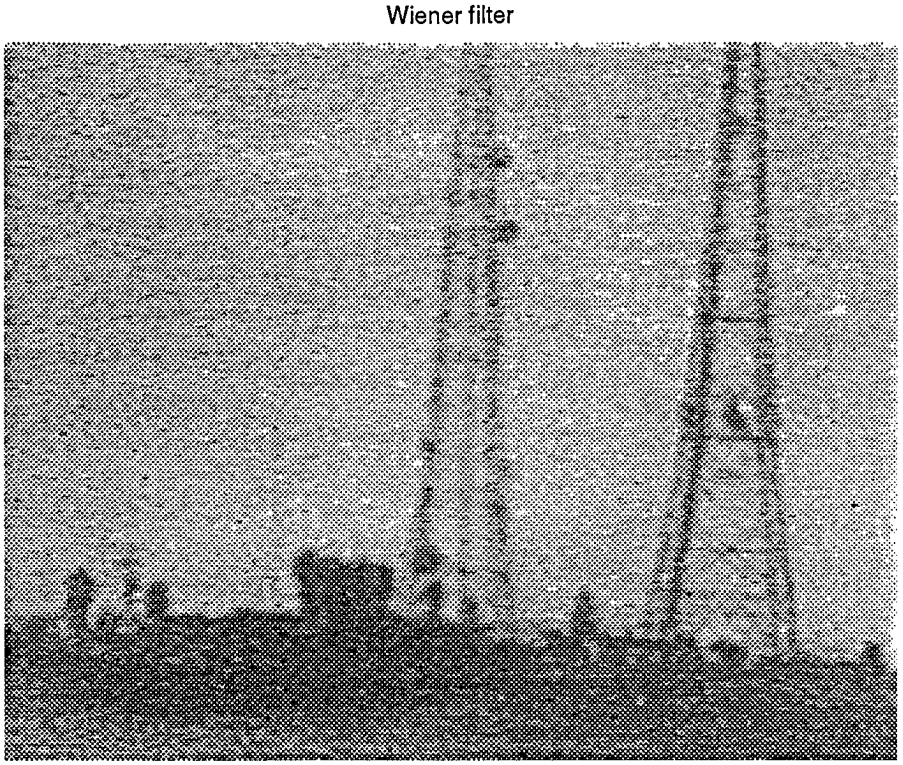
Wiener filter

Fig. 13

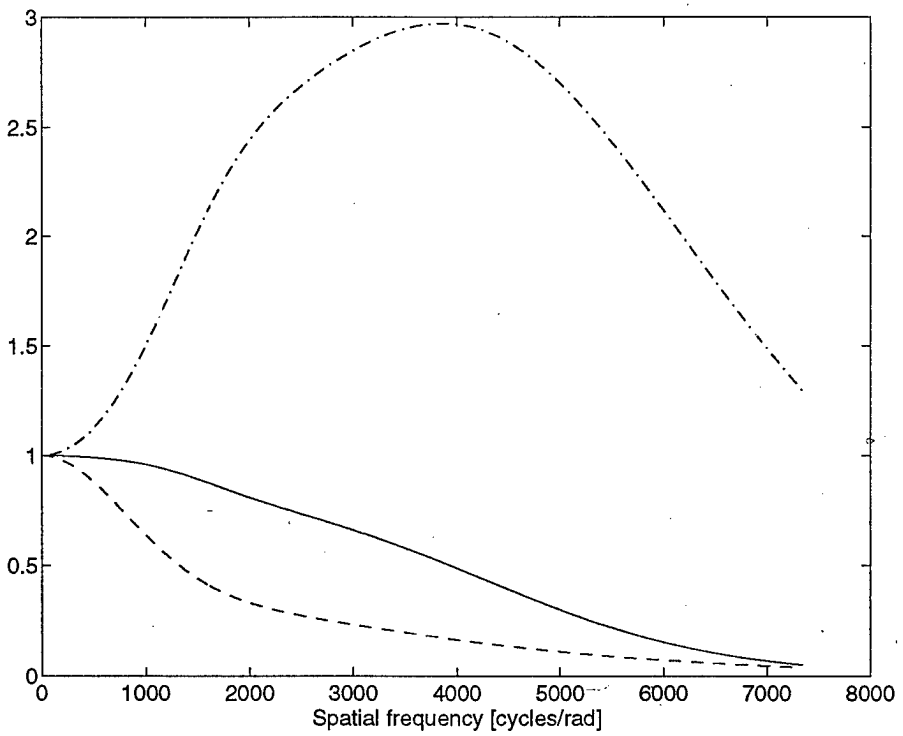
3
2.5
2
1.5
1
0.5
0
0
1000
2000
3000
4000
5000
6000
7000
8000
Spatial frequency [cycles/rad]

Fig. 14

Wiener filter

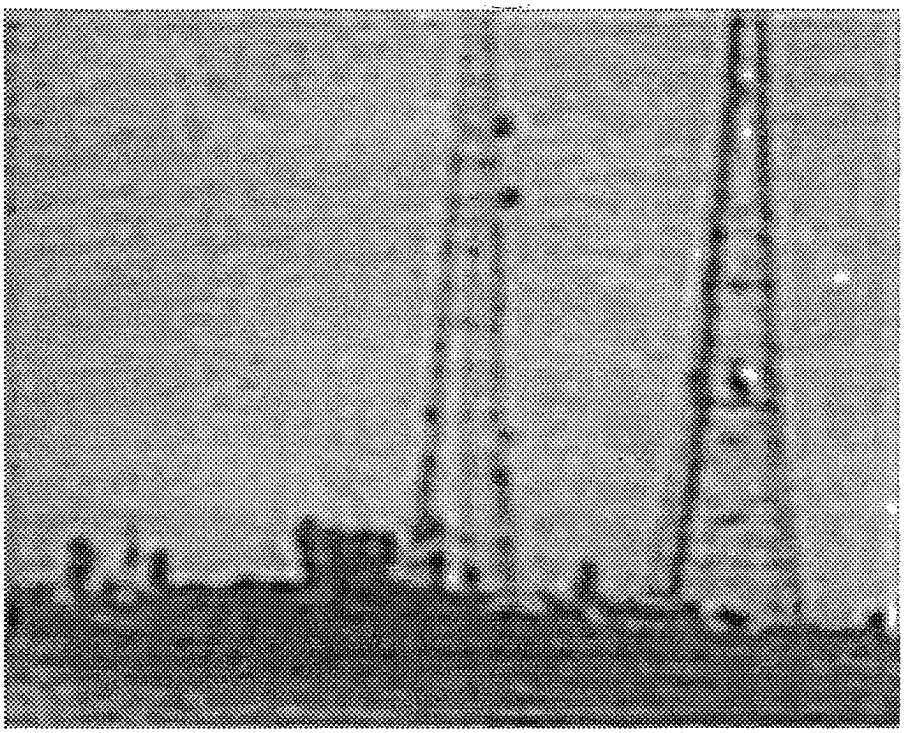

Fig. 15_a

Wiener filter

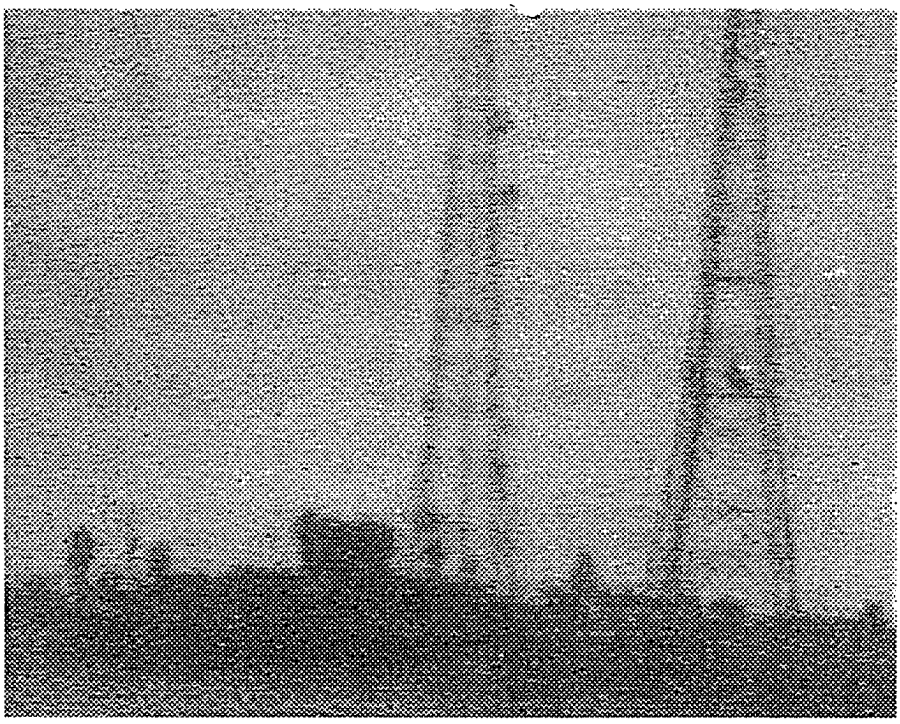

Fig. 15_b

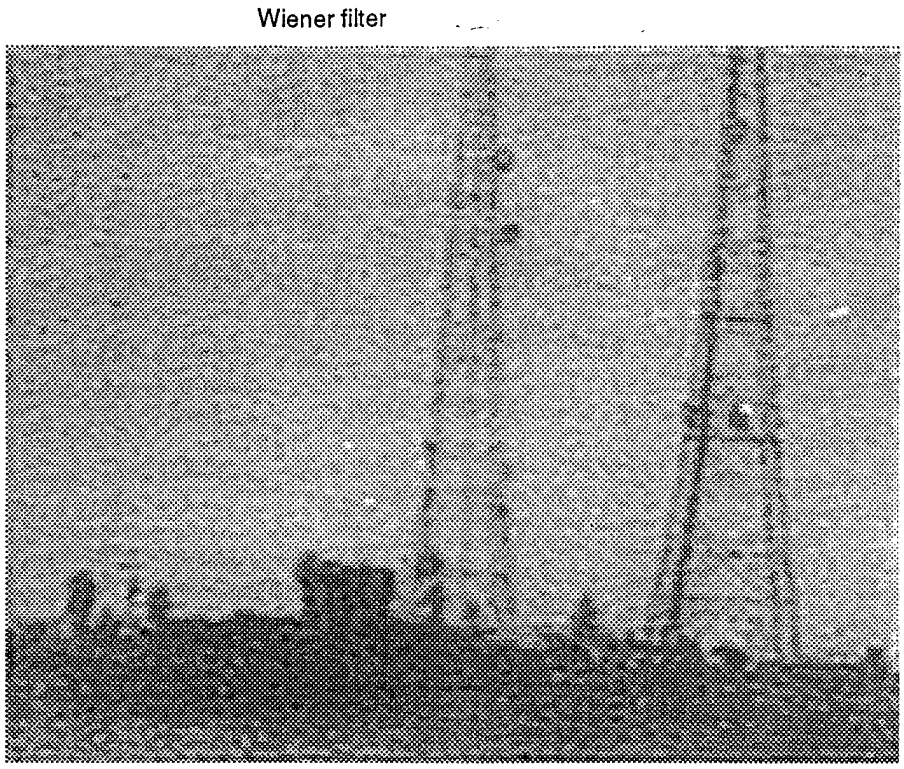
Wiener filter

Fig. 16

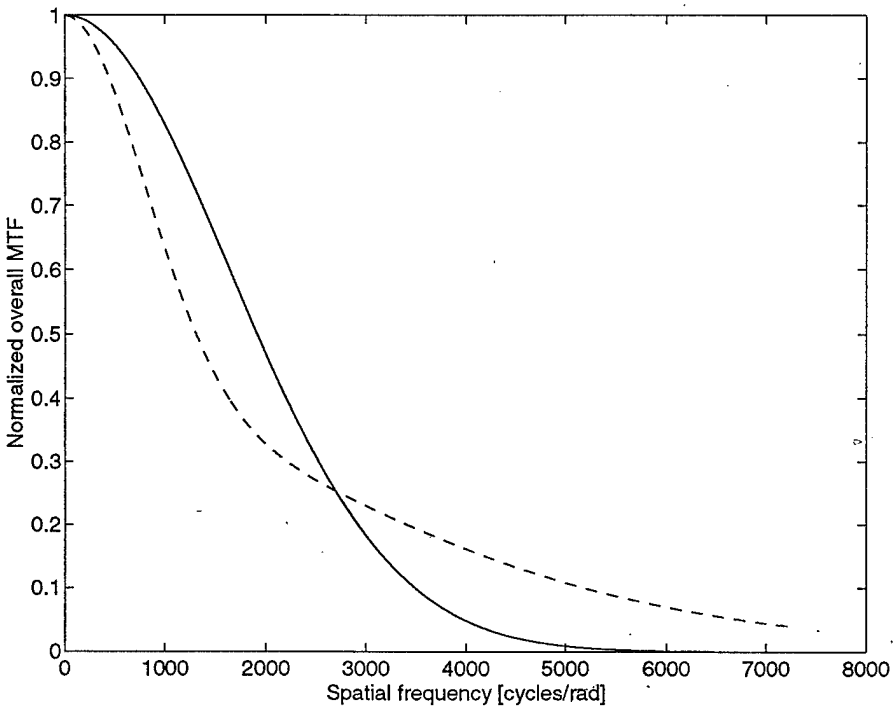
Normalized overall MTF
Spatial frequency [cycles/rad]
0
0.1
0.2
0.3
0.4
0.5
0.6
0.7
0.8
0.9
1
0
1000
2000
3000
4000
5000
6000
7000
8000

Fig. 17

APPENDIX 2

Statistical model for aerosol size distribution parameters according to weather parameters

I. Dror and N. S. Kopeika

Ben Gurion University of the Negev
Department of Electrical and Computer Engineering
Beer Sheva, Israel 84105

ABSTRACT

Predictions of atmospheric transmittance in desert aerosol environments using MODTRAN code diverge significantly from measured data. Good prediction of the desert particulate size distribution is required in order to predict atmospheric scattering and absorption parameters. It is also essential to the prediction of the aerosol atmospheric modulation transfer function which is often the dominant component of the overall atmospheric MTF.[1] Recently[2] an effort to predict desert coarse aerosol statistics but not size distribution according to simple weather parameters has been made. A quantitative analysis of the desert particulate size distribution models was also performed[3]. In this research the size distribution parameters measured by optical counters are related to weather parameters. Known statistical and analytical models such as MODTRAN relate the size distribution parameters only to relative humidity for continental atmospheres. Although humidity has a significant role in the prediction of aerosol size statistics, other weather parameters can also strongly influence the size distribution parameters. Comparisons such as the above can be used to predict under which conditions the MODTRAN aerosol models have good or poor accuracy. It is also hoped that they will lead to improvements in MODTRAN, improving the accuracy of the humidity dependence as well as by incorporating other meteorological parameters into the MODTRAN prediction models.

2. INTRODUCTION

The aerosols that are suspended in the atmosphere are a major factor that influence the quality of images that are propagating through the atmosphere. Scattering and absorption of light rays by the suspended aerosols contribute to the loss of contrast of the received image. Forward light scattering in the direction of the image propagation also reduces the atmospheric modulation transfer function (MTF) and causes actual image blur.

Prediction of the aerosol size distribution can lead to the prediction of the scattering and absorption coefficients and also the scattering phase function of the atmospheric propagating medium. These properties characterize the extinction coefficient of the atmosphere as well as the aerosol MTF of the atmosphere. Models such as that suggested here, and extension of them, can lead to prediction of atmospheric transmission and aerosol derived blur according to weather.

3. EXPERIMENT

The particulate size distribution of the atmosphere was measured over the radius range of 0.16 to 10 μm using a PMS CSASP-100 optical particle counter. The optical counter was located at a height of 25 m

above ground. Integration time of half an hour was chosen and every half hour the average particulate size distribution was recorded. Meteorological parameters were also measured close to the PMS location and the half hour average of the temperature, relative humidity, wind speed, wind direction and solar flux were recorded. The measurements were taken at Ben-Gurion University of the Negev in Beer-Sheva, Israel. Data was collected from June 1991 until March 1994. Both the PMS counter and the Campbell Scientific meteorological station were connected to a personal computer.

Since a goal of this research is to relate the aerosol particulate size distribution parameters to simple weather parameters, the integration times selected for counting and classifying particles according to size have to be shorter than the meteorological time constants. On the other hand, a short integration time can lead to a particulate size distribution curve with insufficient data in which case it is hard to fit the measured data to a known size distribution model. In our measurements an integration time of half an hour was chosen as a compromise between the need for a smooth size distribution curve and the need to measure the aerosol statistics under stationary meteorological conditions.

Fig. 1. describes the changes in the standard deviation of the temperature along a typical summer day. The standard deviation here is calculated on the basis of measurement time periods of half an hour. Fig. 2. shows the changes in the standard deviation of the relative humidity during the same day. These figures show that the most rapid changes occur after sunrise and sunset. In our measurements the standard deviation of the temperature did not exceeded 2°C and that of the relative humidity did not exceeded 5 %. In most of the cases the standard deviations were much less than these values.

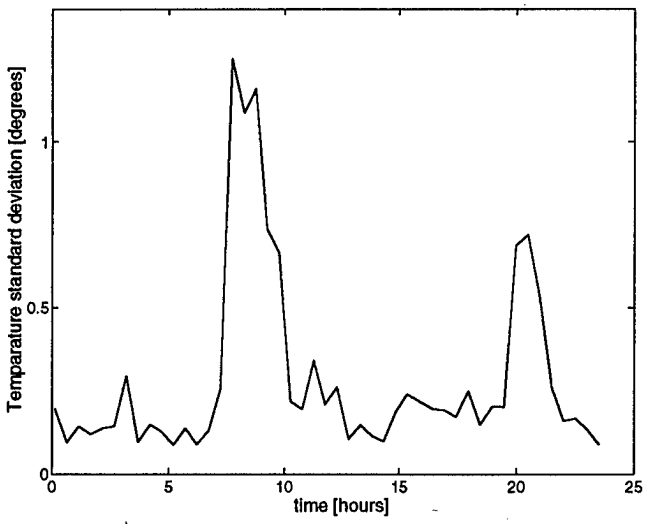

Fig. 1. Half hour standard deviation of the temperature as a function of time during a typical summer day.

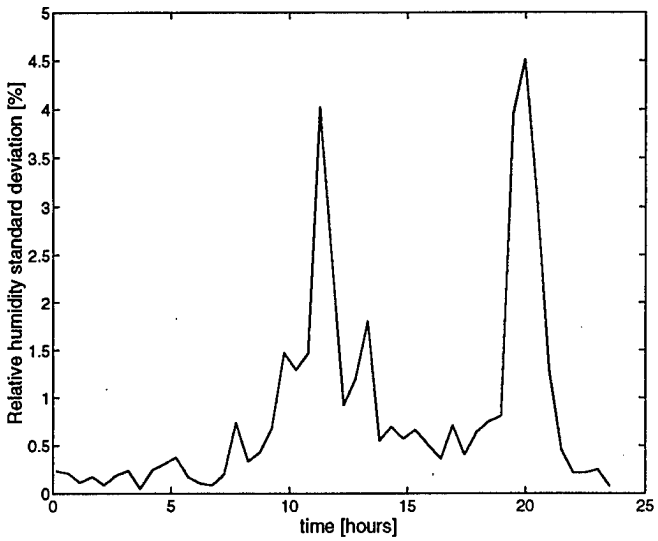

Fig. 2. Half hour standard deviation of the relative humidity as a function of time during a typical summer day.

4. DATA ANALYSIS

The deviations in the aerosol size distribution are large. The sources of the aerosols in the area of our measurements consist of a large variety of aerosol sources. The sources are urban and rural aerosol, marine, haze, industrial and desert dust aerosols that are transferred from two large desert areas during dust storms
from the Sahara desert and from the Saudi Arabian desert.[4]

Fig. 3. describe two extreme aerosol size distribution that were measured during the year 1992. The differences between the two extreme cases is about two orders of magnitude. The lower curve is not continuous because particles at several radii were not counted during an integration period of half an hour. Fig. 4. shows the normalized standard deviation of the measured aerosol radius at each radius over the three year data collection period. The normalized standard deviation of aerosol concentration ranges from 0.5 at a radius of 0.16 μm to 12 at a radius of 10 μm. The aerosol size distribution consists of several distributions that can be modeled by superposition of lognormal distributions.[5] The standard deviation of the particle count is lower at small radii than at large radii since the low mode of the aerosol distribution consists mainly of local aerosols while the large size aerosol population contains also particles that are transported from remote areas. Also the local aerosols are less affected by changes in weather parameters while the larger particles are very sensitive to wind speed and to wind direction which, in some cases, yields information about the remote aerosol source.

A simple size distribution that can characterize the aerosol size distribution is the Junge power law distribution.[6] The size distribution is defined by only two parameters, A and α:

$$dn/dr = A\, r^{-\alpha} \qquad (1)$$

where r is the particle radius and n is the particulate number concentration.

The advantage of this size distribution is that a measured size distribution can be fitted to this model by a simple one variable linear regression.

In our analysis the measured size distributions were fitted to the Junge power law model. Fig. 5. describe the average particulate size distribution and the power law fit. All 6000 measurements of the aerosol size distribution from May 1992 to October 1992 were fitted to the power law distribution and the values of α and A were extracted. The average square of the correlation coefficient R^2 was 0.95.

The power law size distribution parameters A and α were related to the weather parameters that were measured nearby the particulate counter using multiple linear regression analysis. The summer model obtained for A is given by:

$$A = a_0 + a_1 rh + a_2 rh^2 + a_3 rh^3 + a_4 rh^4 \qquad (2)$$

were rh is relative humidity in percents. The coefficients of the model are given in Table 1.

Table 1. Summer model for the prediction of the parameter A.

a_0	a_1	a_2	a_3	a_4
1.917	-0.128	$4.61 \cdot 10^{-3}$	$6.85 \cdot 10^{-5}$	$3.73 \cdot 10^{-7}$

The model obtained for α was the following:

$$\alpha = b_0 + b_1 rh + b_2 rh^2 + b_3 ws \qquad (3)$$

were ws is the average wind speed in $m \cdot s^{-1}$. The coefficients for the prediction of α are given in Table 2.

Table 2. Summer model for the prediction of the parameter α.

b_0	b_1	b_2	b_3
2.68	$2.3 \cdot 10^{-3}$	$8.16 \cdot 10^{-5}$	$-2.65 \cdot 10^{-2}$

The A parameter in this model depends only on the relative humidity. Other dependences were weak and insignificant. α depends also on the average wind speed. Fig. 6 describes the measured α in an ascending order and the modeled α. From this figure it is shown that there is good agreement between the measured parameter and the modeled parameter for about 70% of the measurements. Fig. 7. shows the measured and modeled parameters A in ascending order.

Figs. 8. show some random measured particulate aerosol distributions (solid lines) and the predicted size distribution according to the measured weather parameters (dashed lines). The curves shows that there is very good agreement between the measured data and the model for the parameters α and A for various relative humidity conditions. The straight line represents results (1) - (3) and are not a "best fit" to the measured aerosol size distribution.

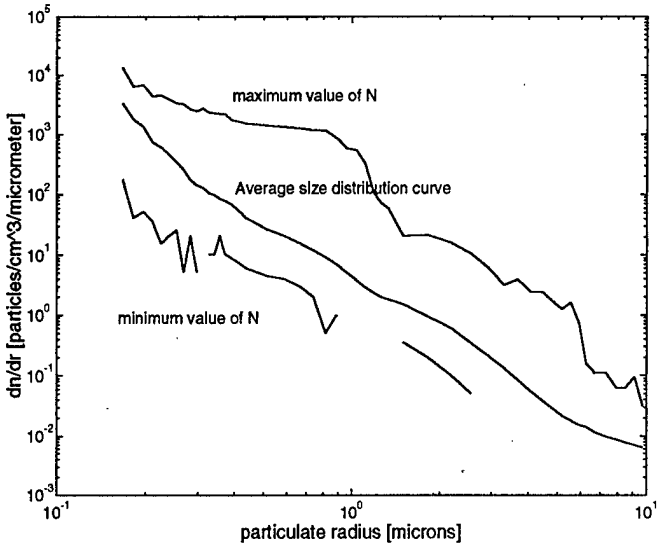

Fig. 3. Average aerosol size distribution curve and size distributions for minimum and maximum numbers of particles that were measured.

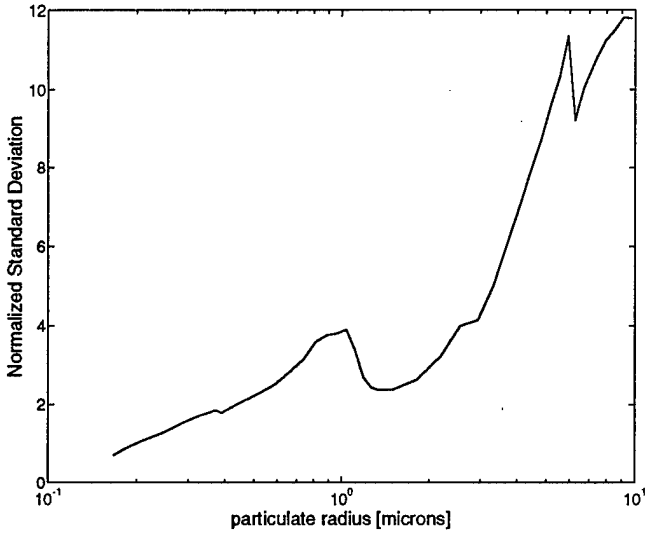

Fig. 4. Standard deviation of all aerosol concentrations normalized according to mean aerosol concentration..

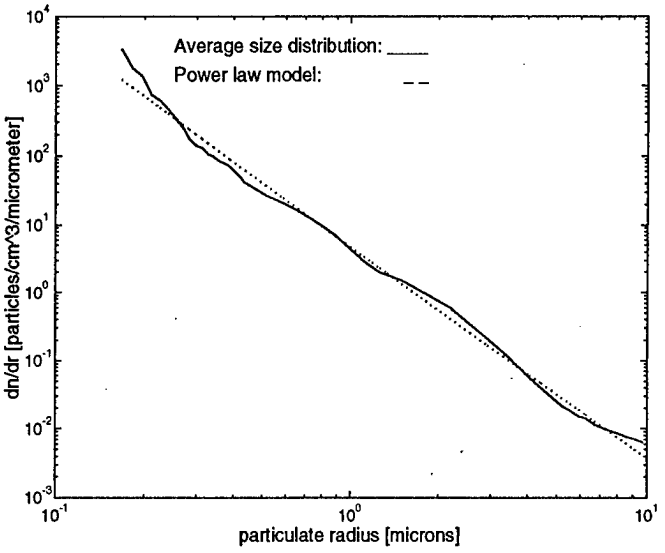

Fig. 5. Measured average particulate size distribution and power law model.

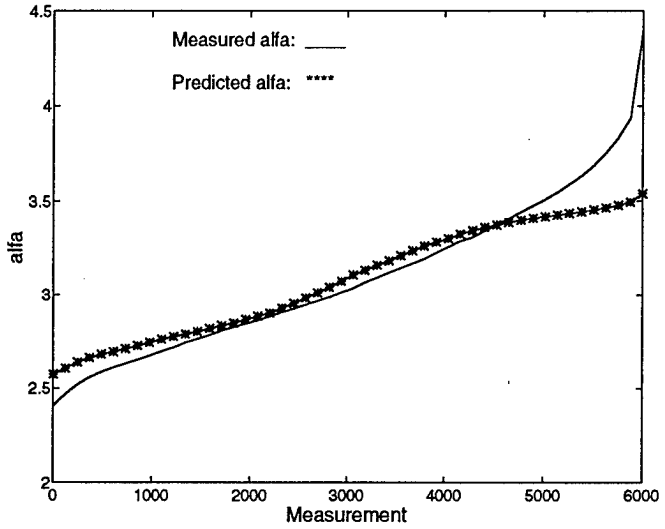

Fig. 6. Comparison of measured and predicted values of α in ascending order.

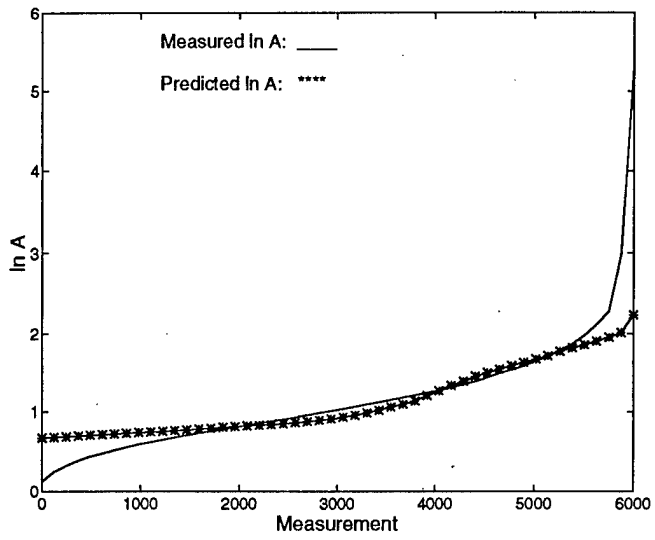

Fig. 7. Comparison of measured and predicted values of A in ascending order.

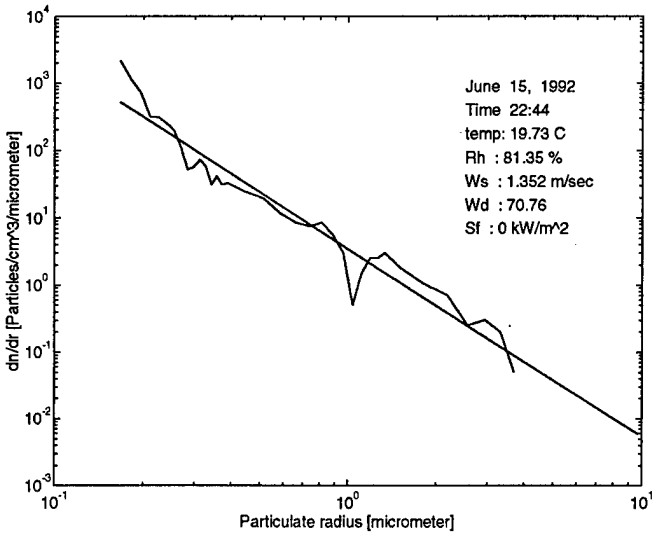

Fig. 8a. Measured and modeled (straight line) size distributions. *Wd* and *Sf* are wind direction and solar flux, respectively.

statistics of the aerosols are influenced strongly by the local weather. There are few exceptions, mainly when the aerosol size distribution consist of transported particles such as desert dust particles or marine particles that are brought from other areas.

For further investigation, the cases when the size distribution curve is affected by remote particles should be studied and the sources of these aerosols should be identified by analysis of the history of the wind speed and wind direction.

6. REFERENCES

1. I. Dror and N. S. Kopeika, "Aerosol and Turbulence MTFs: Comparison Measurements in the Open Atmosphere," *Optics Letters* **17**, 1532-1534, 1992.

2. J. Gottlieb and N. S. Kopeika "Prediction of coarse aerosol statistics according to weather forecast," in *Propagation Engineering: Fourth in a Series,* L. Bissonette and W. B. Miller, eds., *Proc. SPIE,* vol. 1487, pp. 184-191, 1991.

3. I. Dror and N. S. Kopeika, "Prediction of aerosol distribution parameters according to weather forecast," in *Atmospheric Propagation and Remote Sensing*, A. Kohnle and W. Miller, eds., Proc SPIE, vol. 1688, 123-131, 1992.

4. E. Ganor, H. A. Foner, S. Brenner, E. Neeman, and H. Lavi, "The chemical composition of aerosols settling in Israel following dust storms," Atmosph Environment, 25A, No. 12, 2665-2670, 1991.

5. E. P. Shettle and R. W. Fenn, "Models for the aerosols of the lower atmosphere and the effects of humidity variations on their optical properties," AFGL-TR-79-0214, 1979.

6. M. M. R. Williams and S. K. Loyalka, *Aerosol Science*, Chap. 1, Pergamon Press, 1991.